A Modified Simplified Reference Tissue Model for the Quantification of Dopamine $D_{2/3}$ Receptors with [^{18}F]Fallypride Images

Tsartsalis, Stergios; Moulin-Sallanon, Marcelle; Dumas, Noe; Tournier, Benjamin; Ginovart, Nathalie; Millet, Philippe

RESEARCH ARTICLE

A Modified Simplified Reference Tissue Model for the Quantification of Dopamine $D_{2/3}$ Receptors with [^{18}F]Fallypride Images

Stergios Tsartsalis, Marcelle Moulin-Sallanon, Noé Dumas, Benjamin B. Tournier, Nathalie Ginovart, and Philippe Millet

Abstract

Defluorination of [^{18}F]fallypride and accumulation of ^{18}F in skull and glands leads to the contamination of brain structures with spillover activity due to partial volume effects, leading to considerable errors in binding potential estimations. Here we propose a modification of the simplified reference tissue model (SRTM) to take into account the contribution of skull activity to the radioactivity kinetic pattern in cerebellum and target regions. It consists of the introduction of an additional parameter for each volume of interest (s_T) and one for the cerebellum (s_R), corresponding to the fraction of skull activity contaminating these structures. Using five rat positron emission tomography experiments, we applied the modified SRTM (SRTMc), which resulted in excellent fits. As a relative means of comparison of results, we applied factor analysis (FA) to decompose dynamic data into images corresponding to brain and skull activity. With the skull factor images, we estimated the ''true'' s_T and s_R values, ultimately permitting us to fix the s_R value. Parameters obtained with the SRTMc were closely correlated with values obtained from FA-corrected data. In conclusion, we propose an efficient method for reliable quantification of dopamine $D_{2/3}$ receptors with single-injection [^{18}F]fallypride scans that is potentially applicable to human studies where ^{18}F skull accumulation compromises binding parameter estimation.

IN VIVO QUANTIFICATION of dopamine $D_{2/3}$ receptors has been established as an important tool in basic and clinical psychiatric research. [^{18}F]Fallypride, a highly selective dopamine $D_{2/3}$ receptor radioligand, has been widely employed in positron emission tomography (PET) studies of dopaminergic neurotransmission. The potential advantages of its use are its relatively long half-life, its high affinity for both striatal and extrastriatal $D_{2/3}$ receptors, and its sensitivity to amphetamine-induced dopamine release.[1–3] Recent advances in small-animal PET imaging have also permitted in vivo quantification of dopamine $D_{2/3}$ receptors in the context of translational psychiatric research studies in rodents.[4–6]

Nevertheless, the feasibility of reliable $D_{2/3}$ receptor quantification in rodent [^{18}F]fallypride PET studies is limited by a major drawback, which is the spillover activity contamination from the skull and glands. Indeed, defluorination of [^{18}F]fallypride after its injection allows ^{18}F to be rapidly accumulated in the skull and glands. Particularly concerning translational PET neuroimaging, given the limited spatial resolution of small-animal PET scanners and the small size of rodent brain, partial volume effect is relatively large in the rodent cerebral structures under study. These structures are contaminated by the activity due to ^{18}F accumulation in adjacent skull and glands (spillover effect).[7] Spillover activity contamination impairs reliable quantification of $D_{2/3}$ receptors, notably with the use of reference tissue models.[8–10] The reason for this is that the reference region, cerebellum, is one of the most affected.[5]

Partial volume effect correction (PVC) is possible with the application of an algorithm that requires anatomic information from magnetic resonance imaging (MRI)[11] for accurate coregistration of PET and MRI data and tissue segmentation. However, individual MRIs are not always

From the Vulnerability Biomarkers Unit, Division of General Psychiatry, Department of Psychiatry, University Hospitals of Geneva, Geneva, Switzerland; Department of Psychiatry, University of Geneva, Geneva, Switzerland; and INSERM Unit 1039, J. Fourier University, La Tronche, France.

Address reprint requests to: Philippe Millet, PhD, Vulnerability Biomarkers Unit, Division of General Psychiatry, Department of Psychiatry, University Hospitals of Geneva, Switzerland, Chemin du Petit-Bel-Air 2, CH1225, Chêne-Bourg, Switzerland; e-mail: Philippe.Millet@hcuge.ch.

DOI 10.2310/7290.2014.00028

available in small-animal imaging studies. On the other hand, PVC methods that require no anatomic MRI data have been described in human PET studies, but their validity in the case of small-animal PET has not been established.[12] Alternatively, correction of contamination from spillover activity in skull and glands is possible with the application of factor analysis (FA). FA enables decomposition of the signal contained in a series of dynamic images into a few elementary components, among which is the signal due to spillover contamination, which can then be removed. Previously, FA has been employed for the correction of spillover activity contamination in a rat [^{18}F]fallypride imaging study.[5] However, a complex and time-consuming multi-injection experimental protocol with at least a displacement procedure and a total duration of 360 minutes is required to allow biological identification of the components calculated by FA.

Another alternative approach for the correction of spillover activity contamination is the inclusion of spillover correction directly in the compartmental model that is used to fit kinetic PET data.[13] In this article, we adopt this principle to introduce a modified version of the simplified reference tissue model (SRTM),[8,10] that includes parameters for the correction of spillover effects for both volumes of interest (VOI) and reference region directly on raw, single-injection PET images. FA correction of multi-injection data was used in parallel to validate our approach.

Materials and Methods

Animal Preparation

Five male Sprague-Dawley rats (Janvier Laboratories, Le Genet-St-Isle, France) weighing 370 to 400 g were used. PET scanning was performed under isoflurane anesthesia (4% for induction, 2.5% for maintenance). Under anesthesia, a 24-gauge catheter was inserted in the tail vein for radioactive tracer injection. Body temperature was maintained at 37 ± 1°C by means of a thermostatically controlled heating blanket. All experimental procedures were performed in accordance with Swiss federal law on animal care under a protocol approved by the Ethical Committee on Animal Experimentation of the Canton of Geneva, Switzerland.

Experimental Protocol

In the present study, we employed [^{18}F]fallypride (four rats) and [^{18}F]sodium fluoride (hereafter [^{18}F]fluoride) (one rat) multi-injection images from another study published by our group.[5] [^{18}F]Fallypride and [^{18}F]fluoride were obtained from Advanced Accelerator Applications (Thoiry, France). A YAP-(S)PET (ISE, Pisa, Italy) small-animal scanner was employed.[14] Radiotracer was injected over a 1-minute period at a constant volume (0.6 mL) in doses that are presented in Table 1, with an average specific activity (SA) of 118.20 GBq/μmol (injection 1). Injection 2 was performed at 180 minutes, including a mixture of both labeled and unlabeled fallypride (thus a lower SA). Injection 3 was performed at 240 minutes, including only unlabeled fallypride. To demonstrate the effect of pure [^{18}F]fluoride accumulation in skull and glands on brain activity measurement, one rat was imaged using the same protocol as above after injection of [^{18}F]fluoride instead of [^{18}F]fallypride. Dynamic, three-dimensional mode acquisition scans of 360 minutes started immediately after injection of radiotracer with the following protocol: 4 × 0.5 minutes; 3 × 1 minute; 11 × 5 minutes; 12 × 10 minutes; 4 ×

Table 1. Numerical Values of the YAP-(S)PET Protocol Parameters Corresponding to the Five Experiments

Rat	*Duration (min)*	*Injection 1*	*Injection 2*		*Injection 3*	
		*SA**	*Activity/Mass*†	*Activity/Mass*†	*Mass*‡	*Mass*‡
1	360	53.03	43.2/0.295	47.5/0.325	2.00	200.00
2	360	132.96	33.0/0.090	42.7/0.116	2.10	210.00
3	360	169.58	40.2/0.086	46.7/0.099	2.45	245.00
4	360	117.2	38.7/0.120	38.7/0.120	5.00	250.00
5	360	—	5.9/—	6.6/—	5.00	250.00

SA = specific activity.
Experiments 1–4: [^{18}F]fallypride; experiment 5: [^{18}F]fluoride.
*SA (GBq/μmol) of [^{18}F]fallypride at the time of injection. In rat 5, which was injected with [^{18}F]fluoride, no SA is defined.
†Activity/mass (MBq/μg) of [^{18}F]fallypride or [^{18}F]fluoride at the time of injection. In rat 5, only the activity of [^{18}F]fluoride and not mass is given. For injection 2, which consists of a mixture of labeled and unlabeled fallypride (rats 1–4) and [^{18}F]fluoride (rat 5), the Activity/Mass column corresponds to the labeled molecule.
‡Mass of unlabeled molecule (μg). For injection 2, the Mass column refers to the unlabeled molecule.

0.5 minutes; 3 × 1 minute; 11 × 5 minutes; 4 × 0.5 minutes; 3 × 1 minute; 11 × 5 minutes; 6 × 10 minutes.

PET images were reconstructed with a two-dimensional expectation maximization algorithm with single-slice rebinning (50 iterations). The resulting voxel size was 0.5 × 0.5 × 2 mm^3. No postfiltering was applied. Data were corrected for dead time, radioisotope decay, and random counts. No corrections were made for attenuation or scatter.[14] The dynamic PET images were first averaged over time frames between 120 and 180 minutes to enhance visualization of the various structures. These images were manually coregistered to a rat MRI and VOI template[15] that was implemented in *PMOD* software version 3.4 (PMOD Technologies Ltd, Zurich, Switzerland), and the coregistration parameters were employed for dynamic image coregistration. Subsequently, PET images coregistered to the MRI template were used for FA as described below. Time-activity curves (TACs) were generated from VOI in raw and FA-processed dynamic images. We studied 16 different VOI bilaterally and the gray matter in both hemispheres of the cerebellum as a reference region. The VOI were nucleus accumbens, caudate nucleus–putamen, cingulate cortex, medial prefrontal cortex, motor cortex, orbitofrontal cortex, somatosensory cortex, visual cortex, anterior-dorsal hippocampus, posterior hippocampus, hypothalamus, superior colliculus, midbrain, ventral tegmental area, inferior colliculus, and thalamus.

FA of dynamic images was performed using *Pixies* software (Apteryx, Issy-les-Moulineaux, France) on the [^{18}F]fallypride PET images of a multi-injection protocol described in previous work by our group.[5] The reason we followed a multi-injection approach in a study on a reference tissue model is that multi-injection images are necessary for FA application for decomposition of dynamic data into components with distinct biological significance. Then image frames corrected for spillover contamination by means of FA corresponding to the first injection (ie, the first 180 minutes) were employed to obtain non-displaceable binding potential (BP_{ND}) values with the SRTM that provided a means of comparison of the results of the approach we present in this article, which is also performed on images corresponding to the first injection. FA makes the distinct components of a dynamic image more distinguishable. Briefly, it decomposes the signal in a series of dynamic images into a few elementary components[16] and summarizes dynamic images into a finite set of curves (K) termed factors, f_k, and their associated structures, termed factor images, a_k, which represent the spatial distribution of the factors f_k. The original signal $S_i(t)$ associated with pixel i and time t (trixel) can then be expressed through a linear combination of K factors, f_k, weighted by K structures, a_k, using the following relation:

$$S_i(t) = \sum_{k=1}^{K} a_k(i) f_k(t) + e_i(t) \quad (1)$$

where $e_i(t)$ represents the error term for each pixel i at time t, including both noise and modeling errors. It is the remaining part of the image that is not modeled by the factors and structures.

We demonstrated in a previous work on [^{18}F]fallypride that the PET signal measured in rat brain was summarized with the first three orthogonal factors using a positivity constraint on all factors and "an increasing function" on one of the three factors corresponding to ^{18}F skull and gland accumulation.[5] These factors (ie, curves) and the corresponding factor images were computed using the FA algorithm. Factor 1 was identified as the specific binding, factor 2 as the free + nonspecific binding, and factor 3 as the skull accumulation. Three individual dynamic images corresponding to free + nonspecific ($image_{free+nonspe}(t)$), specific ($image_{spe}(t)$), and skull accumulation ($image_{skull}(t)$) can be reconstructed using the FA algorithm.

Consequently, if we consider the modeling error $e_i(t)$ as negligible, the apparent PET image $image^{app}_{PET}(t)$ can be defined as the sum of the three reconstructed dynamic images, the first two of which, when summed, give the image that is free of spillover contamination (FA-corrected image):

$$image^{app}_{PET}(t) = image_{free+nonspe}(t) + image_{spe}(t) + image_{skull}(t) \quad (2)$$

Modified SRTM for Spillover Activity Correction

The time course of radioactivity concentration $C_{PET}(t)$ in a given voxel or VOI, as measured by PET, could be described as follows:

$$C_{PET}(t) = C_{free+nonspe}(t) + C_{spe}(t) \quad (3)$$

where $C_{free+nonspe}(t)$ is the concentration of free ligand and nonspecific binding and $C_{spe}(t)$ is the concentration of specific binding.

In the context of the SRTM,[8,10] we can equally write

$$C_{PET}(t) = SRTM(R_1, k_2, BP, C_r(t)) \quad (4)$$

and

$$C_{PET}(t) = R_1 C_r(t) + [k_2 - R_1 k_2/(1+BP)] C_r(t) \otimes e^{-k_2 t/(1+BP)} \quad (5)$$

with the influx and efflux defined by one–tissue compartment models for the tissue VOI (K_1 and k_2) and for the reference (K'_1 and k'_2). $R_1 = K_1/K'_1$ is the relative delivery. $C_r(t)$ is the concentration in the reference region.

Given that the activity observed in each VOI of the rat brain is contaminated by spillover activity to an extent related to its proximity to extracerebral structures, we delineated a VOI in the skull surrounding the brain to extract a skull TAC, using images of averaged activity between 120 and 180 minutes, where the skull activity is more prominent. This VOI included the "peak skull" voxels that contained > 95% of the maximal activity in the skull.[13] Then apparent TACs extracted from each VOI $C^{app}_{PET}(t)$ of dynamic images can be expressed as the sum of the "true" activity in the VOI $C_{PET}(t)$ and a fraction of the activity in the skull TAC ($s_T * C_{VOI-Skull}(t)$), where s_T is a dimensionless fraction that takes higher values for structures in close proximity to skull and glands and vice versa:

$$C^{app}_{PET}(t) = C_{PET}(t) + S_T C_{VOI\text{-}Skull}(t) \quad (6)$$

Activity in cerebellum $C^{app}_r(t)$, which in [^{18}F]fallypride experiments serves as the reference region, is expressed in a similar manner as the sum of the "true" activity $C_r(t)$ and the corresponding activity due to partial volume effects $S_R C_{VOI-Skull}(t)$ (here the contamination fraction is named s_R):

$$C^{app}_r(t) = C_r(t) + S_R C_{VOI-Skull}(t) \quad (7)$$

So, by combining equations 5, 6, and 7, the modified simplified reference tissue model (SRTMc) equation, with s_T and s_R fitted along with the other parameters, can be expressed as follows:

$$\begin{aligned} C^{app}_{PET}(t) &= R_1\left[C^{app}_r(t) - S_R C_{VOI-Skull}(t)\right] \\ &+ \left[k_2 - R_1 k_2/(1+BP)\right]\left[C^{app}_r(t) - S_R C_{VOI-Skull}(t)\right] \\ &\otimes e^{-k_2 t/(1+BP)} + S_T C_{VOI-Skull}(t) \end{aligned} \quad (8)$$

In addition, from equations 3 and 5, s_T is given by the following equation:

$$S_T(t) = \frac{C^{app}_{PET}(t) - \left(C_{free+non-spe}(t) + C_{Specific}(t)\right)}{C_{VOI-Skull}(t)} \quad (9)$$

Estimation of s Parameters

We also estimated the s_T and s_R fractions in each experimental subject using the FA-derived images. According to equations 2 and 9, we can define an s_T fraction image (or s_R for the value corresponding to cerebellum) as follows:

$$image_{S_T}(t) = \frac{image^{app}_{PET}(t) - \left(image_{free+nonspe}(t) + image_{spe}(t)\right)}{C_{VOI-Skull}(t)} \quad (10)$$

or

$$image_{S_T}(t) = \frac{image_{skull}(t)}{C_{VOI-Skull}(t)} \quad (11)$$

Simulation Study

A simulation study was performed to determine the identifiability of SRTMc parameters and evaluate the reliability of SRTMc to estimate BP_{ND} for various simulated degrees of spillover contamination of VOI and reference region. Free-of-noise TACs corresponding to the 32 VOI were generated from the real FA-corrected data of rat 2 using *PMOD* software. Model curves obtained after fitting FA-corrected data with the SRTM were extracted and used as TACs for further processing. As model curves, these TACs present perfect fits of the SRTM. In addition, as they correspond to FA-corrected data, they have no spillover contamination. Based on equation 8 and using *PMOD*, these TACs were modified to simulate spillover contamination corresponding to various values of s_T (for the 32 VOI) and s_R (for the cerebellum), ranging from 0.05 to 0.30, with 0.05 increments. The skull TAC extracted from the raw image of this particular rat was employed to perform these simulations.

SRTMc was subsequently applied to all 32 VOI. Twenty random Marquardt fits were used in each TAC. To evaluate the identifiability of the parameters of the SRTMc, their correlation matrix was generated after fitting the TACs to the model from the various VOIs in *PMOD*.[17] Alternatively, the SRTMc was also applied with the following configuration: s_R was fixed to the mean value of the four rats obtained as described above. For all combinations of s_T and s_R, the BP_{ND} values obtained were then compared to the corresponding values from the SRTM application to the FA-corrected data of this particular rat. Similarly, the SRTMc-derived s_T values were compared to the "true" ones, that is, the values that were used to simulate the TACs. This aimed at the evaluation of any possible bias induced by the SRTMc, especially when it was applied with a fixed s_R value, taking the difference between the "true" and the fixed s_R value into account.

Data Analysis

Kinetic analysis for binding potential (BP_{ND})[18] estimation in raw images was performed in *PMOD* software where the SRTMc was implemented with an additional module that used nonlinear fitting.[8] This modified version of the SRTM requires fitting two parameters more than for the SRTM, s_T and s_R, which correspond to the degree of spillover activity contamination of VOI and the reference region, respectively. Three parameters are fitted in the original SRTM: R_1, which is the ratio of tracer delivery to VOI (K_1), and reference region (K'_1) k_2 and k'_2, which are the efflux rate constants from the VOI and reference region, respectively.[8] The SRTM was also applied for the estimation of BP_{ND} from FA-corrected images corresponding to the first injection (ie, the first 180 minutes)[5] to provide a means of evaluating the results obtained with the SRTMc.

Images of binding parameters were also created using the pixel-wise modeling tool (PXMOD) in the *PMOD* software,[19] where an additional module for the SRTMc was also implemented using the basis function method for fitting.[20] PXMOD requires a preprocessing stage, that is, performing preliminary calculations such as derivation of initial parameters for the pixel-wise fits. For the SRTMc application, a TAC from a high binding VOI (caudate nucleus–putamen) is fitted using the cerebellum as a reference and the ''spillover'' accumulation TAC, delineated as described above. After preprocessing, pixel-wise calculations of BP_{ND} were performed. To evaluate the robustness of pixel-wise parameter estimation, the VOI template of the Schiffer atlas[15] was used to extract regional BP_{ND} values from parametric images, which were then compared to values obtained from VOI analysis.

Furthermore, we evaluated the minimum duration of scanning required to obtain stable binding parameters. For this reason, the SRTMc was applied on TACs from all VOI over various durations of acquisition starting from the maximal duration (180 minutes) and removing frames of acquisition by 10-minute decrements. For each VOI, we computed the ratio of the BP_{ND} value for a given scan duration to the value corresponding to the maximal duration. An estimation was considered stable in a VOI if the average ratio across all four rats was between 0.95 and 1.05 (ie, within 5% of the value corresponding to 180 minutes) and the standard error was $< 10\%$.

Statistical Analysis

Statistical analysis was performed with XLSTAT software (Addinsoft, NY). Using a Bland-Altman plot and linear regression analysis, we determined whether BP_{ND}, R_1, and s_T values obtained with the SRTMc from raw images were in agreement with those obtained from FA-corrected images. Similarly, to further evaluate how well BP_{ND} values obtained with the SRTMc from raw images and the SRTM from FA-corrected images correlated, we used regression analysis to compare the results in each VOI independently. Similarly, we tested whether BP_{ND} values obtained with pixel-wise application of the SRTMc correlated with the corresponding values from VOI analysis. Differences in BP_{ND} values and in the values of the Akaike information criterion (AIC), a measure of the quality of model fitting to data, obtained for the SRTMc in raw and the SRTM in FA-corrected data were assessed using the paired-samples Student *t*-test. The significance level was set at $p = .05$.

Results

[^{18}F]Fallypride and [^{18}F]Fluoride Brain Distribution and TACs

Figure 1 shows an example of PET images, averaged over 120 to 180 minutes postinjection, coregistered to the MRI atlas in the coronal, sagittal, and horizontal planes. VOI were drawn on a rat MRI template implemented in *PMOD* software. The VOI that corresponds to the spillover activity by the accumulation of [^{18}F]fluoride in the skull for this experimental subject is included.

Representative TACs extracted from raw and FA-corrected [^{18}F]fallypride images and the [^{18}F]fluoride image are presented in Figure 1 (E–G). In rats injected with [^{18}F]fallypride, rapid accumulation of the tracer is observed in all brain structures, followed by a variable clearance rate. Raw images present slow accumulation radioactivity in the skull and glands. As a result, TACs generated from raw images are biased by the spillover activity, an effect mainly observed in later time points corresponding to tracer clearance from brain tissue. In TACs from the FA-corrected image of the same rat, the spillover activity effect is absent and there is an activity decrease pattern in all VOI. Finally, TACs extracted from VOI of the [^{18}F]fluoride image corresponding to the skull accumulation of [^{18}F]fluoride present a slow uptake (as a result of contamination from spillover activity) in all regions. VOI that are closer to the skull and glands (such as the nucleus accumbens, medial prefrontal cortex, orbitofrontal cortex, motor cortex, caudate nucleus–putamen, and cerebellum) are predominantly affected. Others, such as the cingulate cortex and somatosensory cortex, show a moderate level of contamination from spillover activity, whereas the rest of the VOI are less affected.

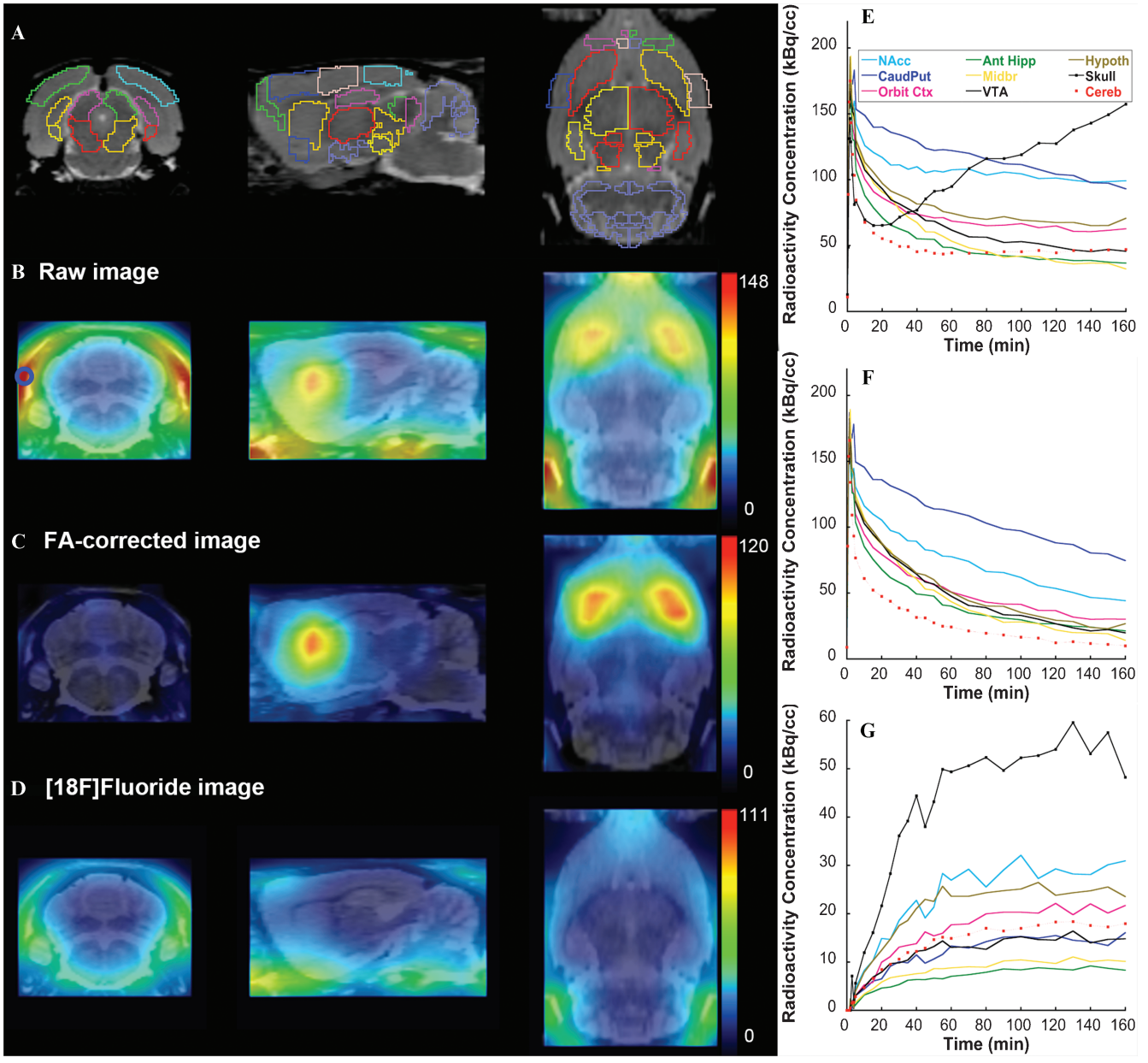

Figure 1. *A*, Representative magnetic resonance image (coronal, sagittal, and axial planes, respectively) with volumes of interest (VOI) used in our study. Averaged PET raw (B), factor analysis (FA)-corrected (C), and [^{18}F]fluoride (D) images obtained between 120 and 180 minutes postinjection 1. Representative time-activity curves obtained from (E) raw, FA-corrected (F) data, and [^{18}F]fluoride images (G). The skull VOI of this particular rat is delineated on the averaged PET image of *B*.

Parameter Estimation from FA

The dynamic images of correction parameters (s) for each VOI were estimated using the FA-derived images and equation 11. This analysis revealed a temporal stability of s parameters, which are shown in Table 2. They range from 0.026 ± 0.014 in the superior colliculus (mean and standard deviations of the values in bilateral VOI across four rats) to 0.386 ± 0.067 in the nucleus accumbens. The s parameter in cerebellum shows little variability across different rats and takes a mean value of 0.214 ± 0.016 (ranging from 0.194 to 0.233).

Simulation Study

We generated noise-free TACs for all 32 VOI and cerebellum, with various levels of simulated spillover activity contamination, that is, s_T and s_R parameters. The SRTMc in its original configuration requires fitting two

Table 2. Mean and Standard Deviations of Parameter Estimates Obtained from Four Experimental Subjects

*VOI**	$BP_{ND\text{-}c}$ †	± *SD*	$BP_{ND\text{-}FA}$ ‡	± *SD*	R_1 §	±*SD*	s_T ‖	± *SD*	s_T ¶	± *SD*
Nucleus accumbens	1.989	1.025	2.417	1.096	1.040	0.241	0.414	0.019	0.386	0.067
Caudate nucleus–putamen	3.331	1.624	3.857	1.732	1.235	0.315	0.349	0.021	0.331	0.122
Cingulate cortex	0.828	0.590	1.130	0.532	1.266	0.404	0.210	0.024	0.161	0.051
Medial prefrontal cortex	1.358	0.729	1.509	0.677	1.399	0.356	0.226	0.016	0.185	0.059
Motor cortex	0.419	0.423	0.826	0.479	1.001	0.311	0.262	0.025	0.220	0.033
Orbitofrontal cortex	0.932	0.580	1.206	0.620	1.077	0.268	0.292	0.022	0.245	0.053
Somatosensory cortex	0.757	0.595	1.197	0.578	1.029	0.213	0.285	0.025	0.253	0.042
Visual cortex	0.220	0.274	0.171	0.165	0.776	0.329	0.185	0.011	0.183	0.030
Anterior-dorsal hippocampus	0.839	0.452	0.825	0.230	1.305	0.268	0.142	0.018	0.111	0.023
Posterior hippocampus	0.729	0.381	0.721	0.236	1.185	0.288	0.201	0.012	0.192	0.031
Hypothalamus	1.230	0.517	1.214	0.444	1.160	0.262	0.283	0.033	0.262	0.066
Superior colliculus	1.373	0.518	0.914	0.229	1.413	0.187	0.046	0.031	0.026	0.014
Midbrain	1.280	0.468	0.904	0.220	1.328	0.209	0.094	0.016	0.073	0.018
Ventral tegmental area	1.173	0.458	0.916	0.240	1.208	0.220	0.167	0.011	0.152	0.035
Inferior colliculus	1.155	0.321	0.785	0.118	1.379	0.175	0.074	0.025	0.059	0.013
Thalamus	1.531	0.633	1.521	0.406	1.389	0.328	0.168	0.017	0.120	0.066

VOI = volume of interest.
*Values refer to the mean of both left and right VOI.
†$BP_{ND\text{-}c}$ (mL/mL) estimated with the modified simplified reference tissue model (SRTMc) in raw data.
‡$BP_{ND\text{-}FA}$ (mL/mL) estimated with the simplified reference tissue model in factor analysis (FA)-corrected data.
§R_1 parameter obtained from SRTMc application in raw data.
‖s_T parameter obtained from SRTMc application in raw data.
¶s_T parameter estimated from factor analysis–derived images.

parameters more than the SRTM, that is, a total of five parameters. Parameter estimation was not possible for any of the VOI with this configuration. Indeed, the correlation matrix of SRTMc parameters (generated in *PMOD*) revealed a high correlation (with *r* values close to unity for all VOIs) between s_T, s_R, and R_1; thus, no further analysis was performed using this configuration. Hence, we tested alternative approaches to simplify the model and enhance the identifiability of the parameters. We examined whether fixing the s_R value, which is common for the application of the SRTMc in all VOI, and fitting the s_T could provide a more robust parameter estimation. The s_R parameter for each rat was obtained above (see Parameter Estimation from FA). For simplicity reasons, a value of 0.2 was fixed and, along with a fitted s_T, was used for further application of the SRTMc.

Next, we evaluated the robustness of kinetic parameter estimation with the SRTMc application using a fixed s_R and fitting s_T. Application of the SRTMc introduces no bias in parameter estimation when the fixed s_R value is identical to the ''true'' one (Figure 2). A small bias (marked as a percentage on lines of Figure 2) in BP_{ND} and values is produced when the fixed s_R value for the application of the SRTMc differs from the ''true'' one. This bias is more prominent as the difference between the fixed s_R (0.2 in these simulation) and the ''true'' s_R augments, up to 13% for high- (eg, 10% for nucleus accumbens and 13% for caudate nucleus–putamen) and less for low-BP_{ND} VOI (eg, 5% for the ventral tegmental area and 3% for the superior colliculus). For a given level of reference tissue contamination from spillover activity (simulated s_R value), the bias is independent of the level of VOI contamination (simulated s_T value). Figure 3 presents the difference between the ''true'' and the fitted s_T value with respect to the application of the SRTMc with a fixed s_R value (at 0.2) for different levels of ''true'' s_R. When the fixed s_R differs from the ''true'' one, fitted s_T differs accordingly from the ''true'' one; thus, the bias in BP_{ND} estimation remains small.

Binding Potential Estimations and Parametric Images

BP_{ND} values were obtained with the SRTMc in raw images and the SRTM in FA-corrected images. For the SRTMc, we used the same configuration as in the simulation study (see above), that is, fixing the s_R parameter to the mean value across the four rats and fitting s_T. The SRTMc presents very good fits, especially compared to SRTM when applied on raw data (Figure 4). Equally, the SRTM application on

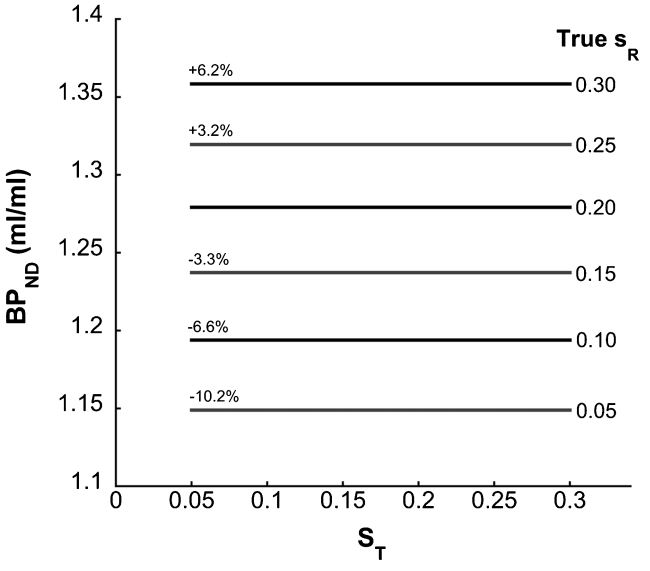

Figure 2. BP_{ND} values obtained from the simulation study. The modified simplified reference tissue model was applied with a fixed s_R at 0.20. True s_T values are plotted on the horizontal axis. *Gray and black lines* represent the BP_{ND} values for various levels of true s_R values. Percentages indicate the error in BP_{ND} estimation induced by the difference between the true s_R value (indicated on the right side) and the fixed one (that is a priori set to 0.2).

FA-corrected data presents good fits. The SRTMc application on raw data is associated with significantly lower mean AIC values across all rats (628.87 for the SRTMc in raw images compared to 637.19 for the SRTM in FA-corrected images, $p < .0001$). The BP_{ND} values obtained with the SRTMc in raw images highly correlate with values obtained with the SRTM in FA-corrected images ($r = .924$, $p < .0001$, Figure 5A) and a Bland-Altman plot reveals no relative systematic bias between these methods (Figure 5B), whereas differences in values obtained with the two methods follow a normal distribution pattern (data not shown). The R_1 values obtained with these models are equally well correlated ($r = .871$, $p < .0001$, Figure 6). Similarly, s_T parameters fitted with the SRTMc took values in good agreement with the values obtained using FA-derived images ($r = .893$, $p < .0001$, Figure 7). The mean parameters for the four experimental subjects are presented in Table 2. Regression analysis of the BP_{ND} values obtained with the SRTMc in raw images and the SRTM in FA-corrected images in each VOI also revealed high correlations. The regression equations and the correlation coefficients are presented in Table 3.

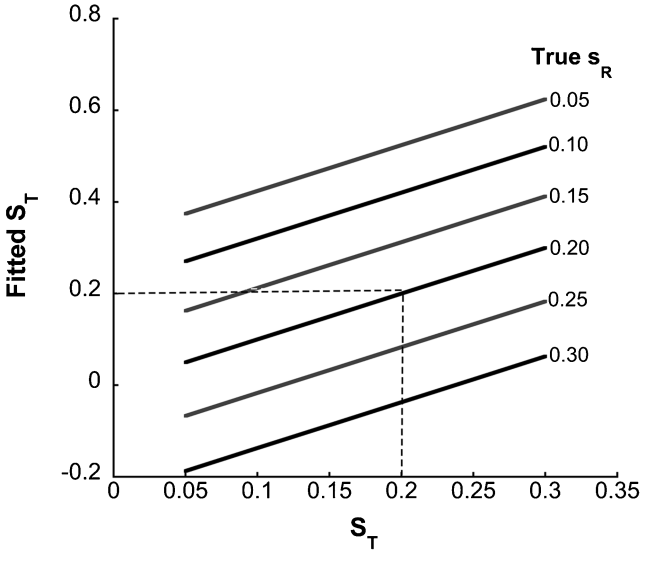

Figure 3. The s_T values obtained from the simulation study. The modified simplified reference tissue model (SRTMc) was applied with a fixed s_R at 0.20. True s_T values are plotted on the horizontal axis. *Gray and black lines* represent the s_T values for various levels of true s_R values. The *dashed line* marks the equality of the fitted s_T value with the true one when the true s_R parameter is fixed for the application of SRTMc.

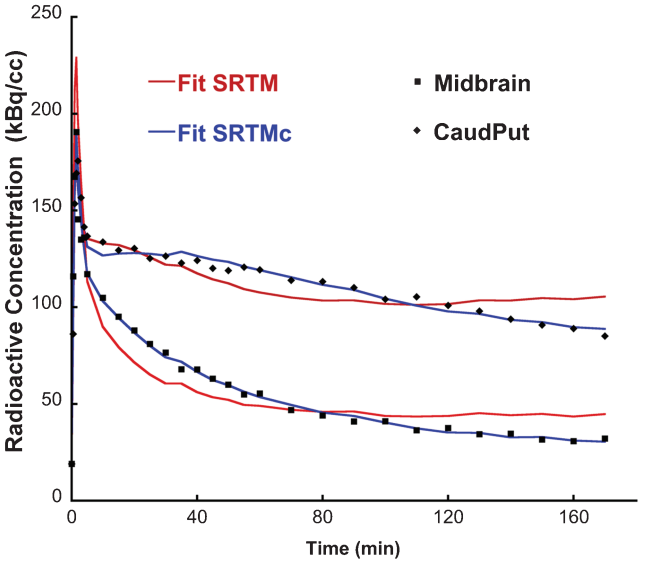

Figure 4. Example of simplified reference tissue model (SRTM) and modified simplified reference tissue model (SRTMc) fits for the caudate nucleus–putamen and midbrain of rat 1.

Parametric images of $BP_{ND\text{-}c}$ with SRTMc in raw data were generated in *PMOD* software (Figure 8). $BP_{ND\text{-}c}$ values obtained by pixel-wise application of the SRTMc were in agreement with the corresponding values obtained with VOI analysis ($r = .970$, $p < .0001$, data not shown). Regarding the minimal scan duration required to obtain stable BP_{ND} parameters, 160 minutes is sufficient to obtain stable values for all VOI, with the exception of somatosensory cortex, where 170-minute scans are required (Table 4).

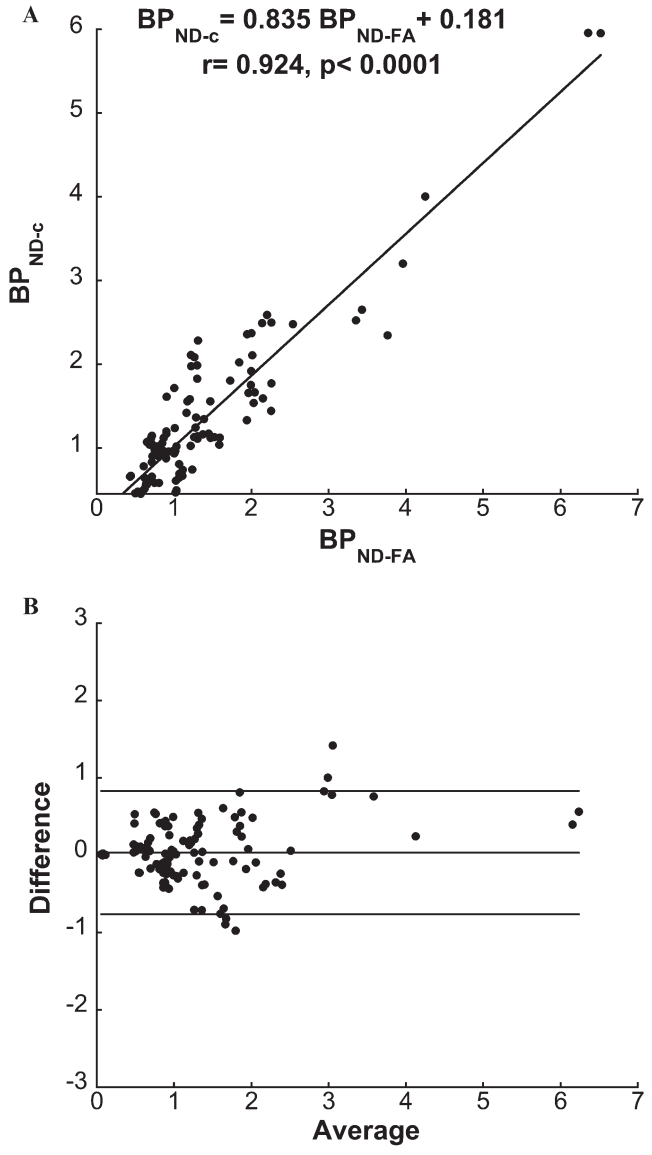

Figure 5. Correlation (A) and Bland-Altman plot (B) of BP_{ND} values estimated with the modified simplified reference tissue model ($BP_{ND\text{-}C}$) on raw images and the simplified reference tissue model ($BP_{ND\text{-}FA}$) on factor analysis (FA)-corrected images, calculated with values of the four experiments, obtained from 32 regions of interest.

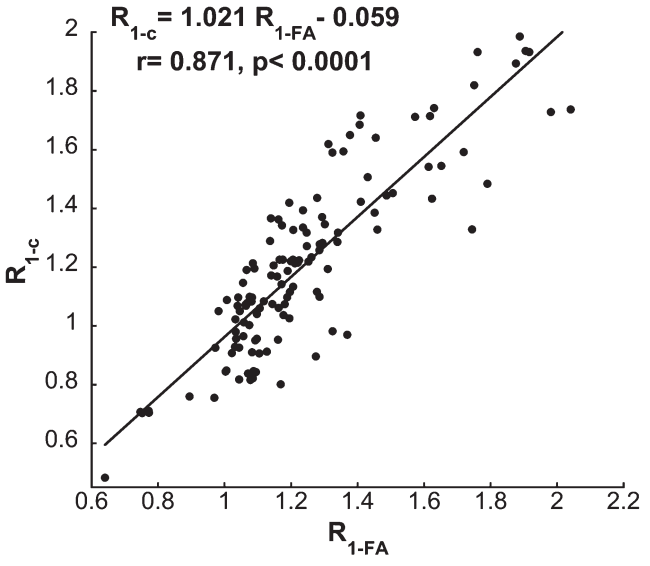

Figure 6. Correlation between R_1 values estimated with the modified simplified reference tissue model ($R_{1\text{-}C}$) on raw images and the simplified reference tissue model ($BP_{1\text{-}FA}$) on factor analysis (FA)-corrected images, calculated with values of the four experiments, obtained from 32 regions of interest.

Discussion

Recent advances in the field of small-animal nuclear neuroimaging have rendered PET a powerful tool of translational neuropsychiatric research. Indeed, [^{18}F] fallypride is a radiotracer widely used in human and small-animal imaging studies of the dopaminergic system.[1–6,21–25] It is a substituted benzamide that binds to $D_{2/3}$ receptors with an affinity that permits quantitative analysis in striatal and extrastriatal brain regions. Nevertheless, fallypride, as an ^{18}F-labeled molecule, is subject to defluorination, giving rise to significant plasma concentrations of free ^{18}F rapidly after tracer injection that accumulates in the skull and glands adjacent to the brain. As a result, partial volume effects account for the perturbation of the radioactivity kinetic pattern in brain structures by skull and gland activity due to

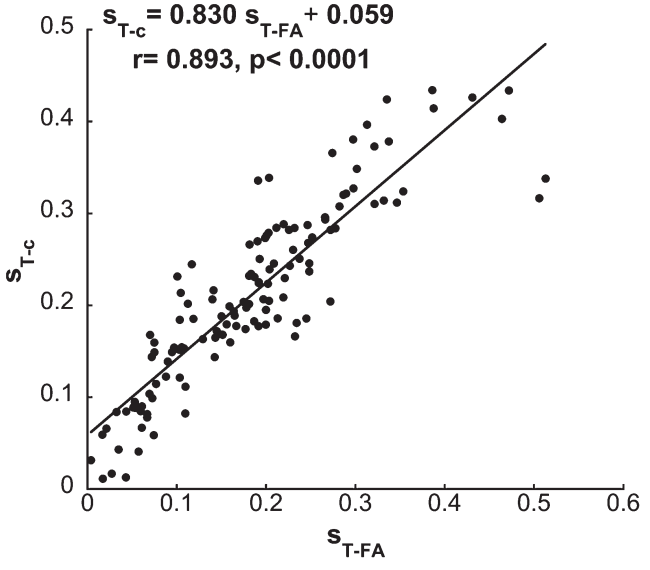

Figure 7. Correlation between s_T values estimated with the modified simplified reference tissue model ($s_{T\text{-}c}$) on raw images and the values that were calculated from the skull factor analysis images ($s_{T\text{-}FA}$), calculated with values of the four experiments, obtained from 32 regions of interest.

Table 3. Regression Analysis Equation and Correlation Coefficients of BP_{ND} Values Obtained with SRTMc Application in Raw and SRTM in FA-Corrected Images in Each VOI

VOI	*C1*[†]	*C2*	*r*[‡]
Nucleus accumbens	0.892	−0.166	.951**
Caudate nucleus–putamen	0.871	−0.026	.929**
Cingulate cortex	1.006	−0.386	.951**
Medial prefrontal cortex	1.000	−0.158	.932**
Motor cortex	0.802	−0.243	.909*
Orbitofrontal cortex	0.902	−0.155	.963***
Somatosensory cortex	0.945	−0.375	.919*
Visual cortex	1.662	−0.064	.999***
Anterior-dorsal hippocampus	1.911	−0.738	.972***
Posterior hippocampus	1.591	−0.418	.987***
Hypothalamus	1.159	−0.177	.996***
Superior colliculus	2.155	−0.597	.953***
Midbrain	2.046	−0.590	.935**
Ventral tegmental area	1.877	−0.546	.985***
Inferior colliculus	2.217	−0.629	.836*
Thalamus	1.541	−0.813	.989***

FA = factor analysis; SRTM = simplified reference tissue model; SRTMc = modified simplified reference tissue model; VOI = volume of interest.
[†]Parameters corresponding to the equation $BP_{ND\text{-}c} = C1*BP_{ND\text{-}FA} + C2$.
[‡]Correlation coefficients.
*$p < .01$; **$p < .001$; ***$p < .0001$.

Table 4. Minimal Scan Duration Required for Stable Outcome Measures of BP_{ND} with SRTMc

VOI	*Minimal Scan Duration (min)*
Nucleus accumbens	160
Caudate nucleus–putamen	160
Cingulate cortex	160
Medial prefrontal cortex	160
Motor cortex	150
Orbitofrontal cortex	160
Somatosensory cortex	170
Visual cortex	120
Anterior-dorsal hippocampus	150
Posterior hippocampus	150
Hypothalamus	160
Superior colliculus	120
Midbrain	120
Ventral tegmental area	140
Inferior colliculus	120
Thalamus	150

SRTMc = modified simplified reference tissue model; VOI = volume of interest.

^{18}F accumulation (spillover activity), particularly in the case of small-animal PET because of the relatively small size of rat and mouse brain structures and the finite spatial resolution of small-animal PET scanners.[5,7]

Spillover activity contamination of rat brain structures leads to important bias in BP_{ND} estimations.[5] Using an [^{18}F]fluoride scan, we demonstrated the degree of contamination of the brain structures. It concerns all brain regions in various levels, depending on their proximity to the skull. One of the structures that are most affected in the rat brain is the cerebellum.[5,22,26] Unbiased cerebellar activity kinetic measurement is very important for the application of the SRTM. It is considered deprived of $D_{2/3}$ receptors; thus, it is used as a reference region for the estimation of nondisplaceable activity. Consequently, any perturbation of activity in the cerebellum biases the binding potential estimation in all VOI. In this study, we used 16 VOI bilaterally. For the majority of VOI, fitting with the SRTM was impossible. In others, its application resulted in very poor fits and aberrant binding potential estimations. Here we introduce a modification to take into account the relative contribution of skull and gland activity in the VOI and cerebellum activity in the brain. We followed the principle that contamination of brain structures due to partial volume effects is a linear function of the activity in the skull scaled by a factor s. We thus incorporated two s parameters in the SRTM, one for each VOI and another for the cerebellum. Appropriate delineation of a skull VOI, representative of skull and gland activity, is the only prerequisite for the application of this modified SRTM.

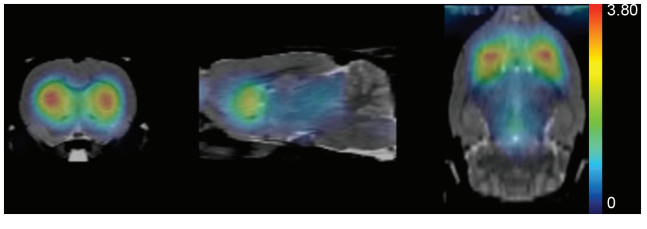

Figure 8. Parametric image of BP_{ND} obtained with the application of the modified simplified reference tissue model in rat 1.

In this study, we exploited the possibilities that FA provides in terms of decomposition of a PET signal to a series of components with a distinct biological significance.[5] The multi-injection protocol that we employed permits distinguishing the signal elements that correspond to (1) specific binding, (2) free + nonspecific binding (ie, the two elements that constitute the exploitable image for kinetic parameter estimation), and (3) skull accumulation of ^{18}F. Using the images consisting of the first two components (more precisely, the image frames corresponding to the first injection of radiotracer), we extracted TACs that were fitted with the SRTM. This provided a

relative means of comparison to evaluate the efficiency of our model in estimating the model parameters (BP_{ND}, R_1). On the other hand, using the skull activity image, we extracted the correction factors (s) for each VOI. This was particularly helpful for the application of the SRTMc as (1) it provided the possibility of knowing the s_R value in advance and (2) it provided another means of comparison for the validation of our model regarding s_T values.

This modified SRTM requires fitting s_T and s_R along with the three parameters of the SRTM.[8] However, due to the high intercorrelation between these two parameters and R_1, we further simplified the model by fixing the s_R value to a mean value across the experimental subjects obtained above using FA-generated images (discussed in Parameter Estimation from FA). Reducing the number of model parameters to be fitted from five to four permitted their identification, regardless of the initial model parameters, as confirmed with the use of random fits in all VOI.

The SRTMc is proposed as a method for binding parameter estimation without the impediment of skull and gland activity. It can be used independently of FA and is only used here as a means of evaluating the model and estimating an s_R value from each rat. The S_R values obtained above present a relatively small variability, and fixing their mean value should not induce any considerable bias to BP_{ND} estimation. To assess this hypothesis, we performed a simulation study using FA-derived TACs (from the specific and free + nonspecific factor images) in which we simulated various levels of contamination. Fixing an s_R value can, indeed, induce an error in parameter estimation. It is proportional to the deviation of the fixed from the ''true'' s_R value and independent of the ''true'' s_T value; that is, it is of the same magnitude for all VOI. So, according to the simulation study and taking into account the low variability of s_R values across rats with similar anatomic characteristics, the error in BP_{ND} estimation should not exceed 3%. That is the error that arises from the SRTMc application with a fixed s_R of 0.2, whereas the ''true'' value is different, positively or negatively, by 0.05. The use of this mean value (0.214) for rat studies could, subsequently, be generalized in the application of the SRTMc in rat [^{18}F]fallypride studies provided that the radiotracer defluorination kinetics present little variability across subjects, rats' anatomic characteristics do not vary considerably (eg, as a result of differences in their age and weight), and, naturally, VOI and reference region delineation is identical. Alternatively, an s_R value could be estimated individually in the following way: initially, the SRTMc is applied in one of the VOI with the lowest s_T fraction, for example, in the superior colliculus. Fixing s_T at zero and fitting s_R should give a value that approximates the ''true'' s_R value. Indeed, to test this hypothesis, we performed a preliminary fit of the SRTMc in the superior colliculus and we estimated a s_R value for each rat. The average value across the four rats was 0.19 (versus 0.21 from Parameter Estimation from FA). They did not differ significantly (by means of a paired-samples *t*-test) from the average s_R value that we used in our estimations (data not shown). However, all binding parameter estimations in this study were performed by fixing the s_R value at 0.214 as described above and in Parameter Estimation from FA.

Employing the SRTMc resulted in very good fits that were found to be significantly better than the fits of the SRTM in FA-corrected data. It provided BP_{ND} and R_1 estimations that were in agreement with those obtained from FA-corrected images. The s_T parameters that were extracted using the skull activity component images from FA correlated with the respective values obtained from the SRTMc. Finally, the SRTMc application in the voxel level resulted in values that closely correspond to these obtained from VOI analysis. Parametric images contain some extracerebral voxels in their foremost part where non-negligible BP_{ND} values are attributed. This is the result of activity other than [^{18}F]fluoride accumulation on lacrimal glands and/or surrounding soft tissue as it is also present (at a very low level) in FA-corrected images (see Figure 1C). It is thus important to note that the SRTMc (as well as FA) corrects biases only due to [^{18}F]fluoride accumulation activity. Radiotracer (even those that do not present defluorination) accumulation in lacrimal glands is indeed a phenomenon to take into account when performing small-animal imaging,[26,27] although of less importance when scanners with better spatial resolution are employed due to the relatively long distance of these glands from the brain. Moreover, it does not degrade the quality of kinetic parameter estimation with the SRTMc, as demonstrated by our results. Skull [^{18}F]fluoride activity accumulation is observed in a closer proximity to the brain and represents by far a more important degrading factor in this kind of study. For this reason, the skull VOI is delineated on images of late frames of acquisition where activity due to [^{18}F]fluoride accumulation predominates.

Examination of BP_{ND} values obtained with the SRTMc in the present study reveals an apparent discrepancy with the results of other rat [^{18}F]fallypride studies in the literature.[22,26–28] Differences in the pattern of reference region and VOI delineation are the cause of this discrepancy. Indeed, in the majority of studies in the

literature, spherical or ellipsoid VOI are placed on the central parts of the anatomic structures under study. Especially in the context of a rat [^{18}F]fallypride study, careful delineation of VOI as far from the skull as possible is essential for the feasibility of kinetic parameter extraction. On the other hand, the definition of brain regions in the Schiffer atlas[15] that we employed in this study closely corresponds to the anatomy of brain regions and thus includes voxels close to the skull that are considerably more affected by spillover contamination than the central ones.

Similarly, a modification of the one–tissue compartment model in an effort to correct the spillover activity contamination was described in a baboon study with [^{18}F]FC, a metabolite of [^{18}F]FCWAY.[13] A skull VOI comprising pixels with an activity superior to the 95% of the maximum radioactivity value in the skull was delineated. Subsequently, the skull TAC was fitted in a two–tissue compartment model of irreversible uptake using plasma [^{18}F] concentration as input function and the spillover term was added in the [^{18}F]FC model equation, adding one more parameter, s, to be fitted in every VOI. Inclusion of pixels with the highest 5% of radioactivity concentration in the skull VOI was proved to be able to give reliable estimations. Diminishing this 5% ''inclusion criterion'' provoked a bias in distribution volume estimations. For this reason, we followed the same principle for skull VOI delineation. On the contrary, as the objective of our study was to use a reference tissue model, we did not measure an input function, whereas we directly used the skull TAC in the SRTMc. The skull TACs of our four rats differ from those extracted from the [^{18}F]fluoride image in the activity pattern that corresponds to the first frames of acquisition. We see a moderately high and rapid increase in the radioactivity concentration, followed by a rapid decrease and, finally, by the slow and constant increase that is due to the ^{18}F accumulation (see Figure 1E). This early increase is probably related to spill-in effects, that is, contamination of the activity pattern in the skull VOI due to the rapid increase in radiotracer concentration in the adjacent brain VOI. To evaluate if this effect could have an effect on binding parameter estimations, we used the FA-derived image that corresponds to the skull activity component: the skull TACs that we extracted from this image for each rat presented this phenomenon to a much lesser degree. Employing these skull TACs in the SRTMc application, instead of those from the raw images, resulted in virtually unchanged parameters (data not shown), indicating that the spill-in effects on the skull TACs do not affect binding potential estimations. Furthermore, another approach for the correction of spillover contamination from skull activity was recently proposed for another $D_{2/3}$ receptor radiotracer, [^{18}F]DMFP.[29] Using a bolus injection plus constant infusion (4-hour) protocol, Mille and colleagues estimated BP_{ND} at the voxel level at equilibrium using the ratio of activity in target voxels to the activity in the cerebellum (VOI).[29] Activity in the cerebellum was corrected for spillover activity from nearby skull with a scaling factor whose median value was found to be 0.009, whereas no correction for target regions was considered. Nevertheless, correction for target regions is necessary in the case of the SRTMc described in the present study for all but a few VOI, which are naturally much less affected from skull activity contamination due to their position (eg, the superior colliculus). The difference in the scaling parameter value for the cerebellum between this study and ours, as well as the need for introduction of a correction parameter for each VOI in the SRTMc, might possibly lie in the employment of different radiotracers and in the pattern of VOI delineation in the two studies.

The SRTMc that we propose here could be employed as an alternative to other approaches for PVC related to skull activity. PVC is an established and widely used method employed successfully in the case of spillover activity from adjacent cerebral structures. A prerequisite for its application is a precise tissue segmentation using MRI data that, in the case of skull and gland spillover activity affects correction, would need a meticulous definition of these regions.[5,7,30,31] On the other hand, FA correction for skull and gland activity, which we described in a previous article,[5] is a powerful tool when applied on images with a multi-injection protocol (which was particularly valuable for the present study). In the case of single-injection studies, it can be used for data denoising,[32] but distinguishing different biologically meaningful components cannot be very efficient: the principle of the FA is the distinction of a finite number of dynamic image components based on the temporal pattern of kinetics. A multi-injection protocol with a second injection of a low specific activity tracer dose and a third injection of cold compound only permits distinguishing the biologically distinct components of the signal: the skull accumulation, that is, the component that is constantly augmenting and is not displaceable; the free and nonspecific binding, that is, the component that is nondisplaceable but not augmenting either; and the one corresponding specific binding, that is, the displaceable component. Indeed, using this protocol, differences in the kinetic patterns of these components are readily distinguishable. A single-injection scan lacks this information as all three components do not present considerable

differences in their kinetic patterns. The SRTMc application is associated with the advantage that a relatively simple 160-minute scan protocol of a single-[^{18}F]fallypride injection is sufficient to permit BP_{ND} estimations with the SRTMc. Interestingly, another approach to diminish the effect of skull activity on binding potential estimations using the SRTM could be the employment of another reference region.[33] However, partial volume effect due to tracer defluorination is not the only factor contributing to brain activity contamination. Other factors and, notably, scattered photons may equally have a considerable impact, particularly in the cerebellum.[34]

Conclusion

We propose a modified version of the SRTM that takes into account spillover activity contamination due to tracer defluorination and subsequent ^{18}F accumulation in the skull and glands. The modification consists of the introduction of scaling factors that indicate the relative contribution of skull activity (as delineated by a skull VOI) to all brain regions. This model permits binding potential estimation from single-injection studies, is simple to employ in the VOI or voxel level, and is applicable, after thorough evaluation using similar-design studies, to human studies with fluorinated radiotracers where ^{18}F skull accumulation compromises binding parameter estimation.

Acknowledgments

Financial disclosure of authors: This work was supported by the Swiss National Science Foundation (grant no. 310030_120369). The authors are grateful for the contributions of the BioPark in Archamps, France, the Fondation Caisse d'Epargne Rhône-Alpes, the ABC Laboratory of the European Scientific Institute, and the "Association IFRAD Suisse," which was created in 2009 at the initiative of the "Fondation pour la Recherche sur Alzheimer" (formerly IFRAD France). S.T. received a scholarship from the Greek National Scholarship Foundation.

Financial disclosure of reviewers: None reported.

References

1. Christian BT, Narayanan TK, Shi B, Mukherjee J. Quantitation of striatal and extrastriatal D-2 dopamine receptors using PET imaging of [(18)F]fallypride in nonhuman primates. Synapse 2000;38:71–9, doi:10.1002/1098-2396(200010)38:1<71::AID-SYN8>3.0.CO;2-2.
2. Mukherjee J, Christian BT, Narayanan TK, et al. Measurement of d-amphetamine-induced effects on the binding of dopamine D-2/D-3 receptor radioligand, 18F-fallypride in extrastriatal brain regions in non-human primates using PET. Brain Res 2005;1032:77–84.
3. Slifstein M, Hwang DR, Huang Y, et al. In vivo affinity of [18F]fallypride for striatal and extrastriatal dopamine D2 receptors in nonhuman primates. Psychopharmacology 2004;175:274–86, doi:10.1007/s00213-004-1830-x.
4. Ginovart N, Tournier B, Moulin-Sallanon M, et al. Chronic Δ9-tetrahydrocannabinol exposure induces a sensitization of dopamine D2/3 receptors in the mesoaccumbens and nigrostriatal systems. Neuropsychopharmacology 2012;37:2355–67, doi:10.1038/npp.2012.91. [Epub 2012 Jun 13]
5. Millet P, Moulin-Sallanon M, Tournier BB, et al. Quantification of dopamine D(2/3) receptors in rat brain using factor analysis corrected [18F]fallypride images. Neuroimage 2012;62:1455–68, doi:10.1016/j.neuroimage.2012.05.075.
6. Tournier BB, Steimer T, Millet P, et al. Innately low D2 receptor availability is associated with high novelty-seeking and enhanced behavioural sensitization to amphetamine. Int J Neuropsychopharmacol 2013;16:1–16.
7. Rousset OG, Zaidi H. Correction for partial volume effects in emission tomography. In: Zaidi H, editor. Quantitative analysis in nuclear medicine imaging. New York: Springer US; 2005. p. 236–71.
8. Lammertsma AA, Hume SP. Simplified reference tissue model for PET receptor studies. Neuroimage 1996;4:153–8, doi:10.1006/nimg.1996.0066.
9. Logan J, Fowler JS, Volkow ND, et al. Distribution volume ratios without blood sampling from graphical analysis of PET data. J Cereb Blood Flow Metab 1996;16:834–40, doi:10.1097/00004647-199609000-00008.
10. Wu Y, Carson RE. Noise reduction in the simplified reference tissue model for neuroreceptor functional imaging. J Cereb Blood Flow Metab 2002;22:1440–52, doi:10.1097/00004647-200212000-00004.
11. Meltzer CC, Kinahan PE, Greer PJ, et al. Comparative evaluation of MR-based partial-volume correction schemes for PET. J Nucl Med 1999;40:2053–65.
12. Tohka J, Reilhac A. Deconvolution-based partial volume correction in raclopride-PET and Monte Carlo comparison to MR-based method. Neuroimage 2008;39:1570–84, doi:10.1016/j.neuroimage.2007.10.038.
13. Carson RE, Wu Y, Lang L, et al. Brain uptake of the acid metabolites of F-18-labeled WAY 100635 analogs. J Cereb Blood Flow Metab 2003;23:249–60, doi:10.1097/00004647-200302000-00012.
14. Del Guerra A, Bartoli A, Belcari N, et al. Performance evaluation of the fully engineered YAP-(S)PET scanner for small animal imaging. IEEE Trans Nucl Sci 2006;53:1078–83.
15. Schiffer WK, Mirrione MM, Biegon A, et al. Serial microPET measures of the metabolic reaction to a microdialysis probe implant. J Neurosci Methods 2006;155:272–84, doi:10.1016/j.jneumeth.2006.01.027.
16. Di Paola R, Bazin JP, Aubry F, et al. Handling of dynamic sequences in nuclear medicine. IEEE Trans Nucl Sci 1982;NS29,1310–21.
17. Graham MM. Kinetic evaluation using sensitivity functions and correlation matrices [abstract]. J Nucl Med 1995;36:1208.
18. Innis RB, Cunningham VJ, Delforge J, et al. Consensus nomenclature for in vivo imaging of reversibly binding radioligands. J Cereb Blood Flow Metab 2007;27:1533–9, doi:10.1038/sj.jcbfm.9600493.

19. PXMOD pixel-wise modeling tool user's guide. Zurich: PMOD Technologies; 2012.
20. Gunn RN, Lammertsma AA, Hume SP, Cunningham VJ. Parametric imaging of ligand-receptor binding in PET using a simplified reference region model. Neuroimage 1997;6:279–87, doi:10.1006/nimg.1997.0303.
21. Christian BT, Narayanan T, Shi B, et al. Measuring the in vivo binding parameters of [18F]-fallypride in monkeys using a PET multiple-injection protocol. J Cereb Blood Flow Metab 2004;24: 309–22, doi:10.1097/01.WCB.0000105020.93708.DD.
22. Constantinescu CC, Coleman RA, Pan ML, Mukherjee J. Striatal and extrastriatal microPET imaging of D2/D3 dopamine receptors in rat brain with [(1)(8)F]fallypride and [(1)(8)F]desmethoxyfallypride. Synapse 2011;65:778–87, doi:10.1002/syn.20904.
23. Mukherjee J, Christian BT, Narayanan TK, et al. Evaluation of dopamine D-2 receptor occupancy by clozapine, risperidone, and haloperidol in vivo in the rodent and nonhuman primate brain using 18F-fallypride. Neuropsychopharmacology 2001;25:476–88, doi:10.1016/S0893-133X(01)00251-2.
24. Choi JY, Kim CH, Jeon TJ, et al. Evaluation of dopamine transporters and D2 receptors in hemiparkinsonian rat brains in vivo using consecutive PET scans of [18F]FPCIT and [18F]fallypride. Appl Radiat Isot 2012;70:2689–94, doi:10.1016/j.apradiso.2012.08.005.
25. Mukherjee J, Yang ZY, Brown T, et al. Preliminary assessment of extrastriatal dopamine D-2 receptor binding in the rodent and nonhuman primate brains using the high affinity radioligand, 18F-fallypride. Nucl Med Biol 1999;26:519–27.
26. Yoder KK, Mock BH, Zheng QH, et al. Assessment of i.p. injection of [18F]fallypride for behavioral neuroimaging in rats. J Neurosci Methods 2011;196:70–5, doi:10.1016/j.jneumeth.2010.12.027.
27. Tantawy MN, Peterson TE, Jones CK, et al. Impact of isoflurane anesthesia on D2 receptor occupancy by [18F]fallypride measured by microPET with a modified Logan plot. Synapse 2011;65:1173–80, doi:10.1002/syn.20955.
28. Tantawy MN, Jones CK, Baldwin RM, et al. [(18)F]Fallypride dopamine D2 receptor studies using delayed microPET scans and a modified Logan plot. Nucl Med Biol 2009;36:931–40, doi:10.1016/j.nucmedbio.2009.06.007.
29. Mille E, Cumming P, Rominger A, et al. Compensation for cranial spill-in into the cerebellum improves quantitation of striatal dopamine D(2)/(3) receptors in rats with prolonged [(1)(8)F]-DMFP infusions. Synapse 2012;66:705–13, doi:10.1002/syn.21558.
30. Hayakawa N, Uemura K, Ishiwata K, et al. A PET-MRI registration technique for PET studies of the rat brain. Nucl Med Biol 2000;27: 121–5, doi:10.1016/S0969-8051(99)00098-0.
31. Muller-Gartner HW, Links JM, Prince JL, et al. Measurement of radiotracer concentration in brain gray matter using positron emission tomography: MRI-based correction for partial volume effects. J Cereb Blood Flow Metab 1992;12:571–83, doi:10.1038/jcbfm.1992.81.
32. Tsartsalis S, Moulin-Sallanon M, Dumas N, et al. Quantification of GABAA receptors in the rat brain with [(123)I] Iomazenil SPECT from factor analysis-denoised images. Nucl Med Biol 2014;41:186–95, doi:10.1016/j.nucmedbio.2013.11.008.
33. Ishibashi K, Robertson CL, Mandelkern MA, et al. The simplified reference tissue model with [^{18}F]fallypride positron emission tomography: choice of reference region. Mol Imaging 2013;12(8). DOI: 10.2310/7290.2013.00065.
34. Vandervoort E, Camborde ML, Jan S, Sossi V. Monte Carlo modelling of singles-mode transmission data for small animal PET scanners. Phys Med Biol 2007;52:3169–84, doi:10.1088/0031-9155/52/11/016.